Vol 14 No 4, April 2005
1009-1963/2005/14(04)/0838-06
Chinese Physics
© 2005 Chin. Phys. Soc.
and IOP Publishing Ltd

Modelling the crystal growth in highly undercooled alloy melts by non-isothermal phase-field method*

Li Mei-E(李梅娥)[a)†], Yang Gen-Cang(杨根仓)[b)], and Zhou Yao-He(周尧和)[b)]

[a)] *School of Material Science and Engineering, Xi'an Jiaotong University, Xi'an 710049, China*

[b)] *State Key Laboratory of Solidification Processing, Northwestern Polytechnical University, Xi'an 710072, China*

(Received 23 July 2004; revised manuscript received 2 October 2004)

A non-isothermal phase-field model is used to simulate the rapid solidification of highly undercooled alloy melts. The influence of undercooling on the solidification process is studied. It is indicated that with the increase of undercooling, the dendrite morphology changes from poorly developed dendrite, via the well-developed dendrite containing secondary and ternary arms, to the compact diamond-shaped grain. With increasing undercooling, the tip radius changes in the following rule: decrease → increase → decrease while the growth velocity increases constantly, which is consistent with the results predicted by the Boettinger–Coriell–Trivedi model. The thermal, solutal and kinetic undercooling contributions under different initial undercooling are also determined. It is shown that when the undercooling is increased beyond a certain value, the thermal undercooling contribution exceeds the solutal contribution and the dendrite growth transits from solutal diffusion controlled to thermal diffusion controlled one.

Keywords: high undercooling, non-isothermal phase-field method, dendrite morphology, operating state of dendrite tip

PACC: 8130, 6150C, 7115Q, 8140

1. Introduction

High undercooling technique plays an important role in modern theoretical research of solidification. Rapid solidification of highly undercooled melts deviates severely from equilibrium thermodynamics, which makes the nucleation mechanism, the mode of crystal growth and the material properties change dramatically.

In addition to a great deal of experimental research, several theoretical models describing the crystal growth in undercooled melts have been proposed. Lipton, Glicksman and Kurz[1] built the crystal growth model (LGK model) at low undercoolings. Lipton, Kurz and Trivedi[2] extended this model to the rapid solidification of deeply undercooled melts regarding the solute trapping effect (LKT model). Boettinger, Coriell and Trivedi[3] took the interface kinetic effect into account and put forward the most perfect model so far for crystal growth in undercooled melts (BCT model). Despite the above achievements, there are still many limitations in the experimental and theoretical researches. For example, the largest undercooling that can be obtained is limited by the capability of experimental equipments and a lot of assumptions must be introduced in the derivation of the theoretical models. Therefore, it is a natural choice to have recourse to numerical computations.

Due to the ability to produce realistic dendrite morphologies, phase-field method has been widely used to model the phase transformations and the accompanying microstructure evolution in recent years. But its application to modelling the solidification of metallic materials has been so far mostly limited to non-isothermal solidification of pure metals or isothermal solidification of binary alloys.[4−7] In order to model the rapid solidification of highly undercooled alloy melts, however, it is essential to adopt the non-isothermal phase-field model because thermal diffusion is an important factor influencing the crystal growth.

In this paper, we use a non-isothermal phase-field model to study the influence of undercooling on dendrite morphologies with the realistic physical pa-

*Project supported by the National Natural Science Foundation of China (Grant Nos 50395103 and 50271057) and by the fund of the State Key Laboratory of Solidification Processing in NPU, China.

†E-mail: limeie@mail.xjtu.edu.cn

rameters adopted. In addition, the dendrite tip radius, the growth velocity and the solutal, the thermal, the kinetic undercooling contributions at different initial undercoolings are determined from the simulation. The results are compared with that given by the BCT model and good agreement is obtained.

2. Computational procedure

2.1. Phase-field model

The phase-field model is based on the following entropy functional[8]:

$$S = \int [s(e,\phi,c) - \frac{\varepsilon^2}{2}|\nabla\phi|^2]\mathrm{d}v, \tag{1}$$

where s is the entropy density that depends on internal energy e, phase field variable ϕ and concentration c. The second term in the integrand is a gradient correction to s. To ensure a positive entropy production, the governing equation for the phase field can be written as

$$\dot{\phi} = M_\phi \frac{\delta S}{\delta \phi}. \tag{2}$$

The evolution of the other two variables, e and c, is given by the conservation laws and the irreversible thermodynamics linear laws as

$$\dot{c} = -\nabla \cdot \left(M_c \nabla \frac{\delta S}{\delta c} \right), \tag{3}$$

$$\dot{e} = -\nabla \cdot \left(M_e \nabla \frac{\delta S}{\delta e} \right), \tag{4}$$

in which M_ϕ, M_c, M_e are positive constants. Evaluating the functional derivatives yields the following governing differential equations:

$$\frac{\partial \phi}{\partial t} = M_\phi[\nabla \cdot (\varepsilon^2 \nabla\phi) - (1-c)H^A - cH^B], \tag{5}$$

$$\begin{aligned}\frac{\partial c}{\partial t} =& -\nabla \cdot [-D_c \nabla c + M_c(H^A - H^B)\nabla\phi \\ &+ M_c \cdot \Psi(\phi,T)\nabla T],\end{aligned} \tag{6}$$

$$\begin{aligned}\frac{\partial T}{\partial t} =& D_\mathrm{T}\nabla^2 T - \frac{(1-c)L^A + cL^B}{C_\mathrm{P}} \\ &\cdot P'(\phi)\cdot \frac{\partial \phi}{\partial t} + \frac{L^A - L^B}{C_\mathrm{P}} P(\phi)\frac{\partial c}{\partial t},\end{aligned} \tag{7}$$

where H^A, H^B and $\Psi(\phi,T)$ are defined as

$$H^A = P'(\phi)L^A\left(\frac{1}{T} - \frac{1}{T_\mathrm{m}^A}\right) + W^A g'(\phi), \tag{8}$$

$$H^B = P'(\phi)L^B\left(\frac{1}{T} - \frac{1}{T_\mathrm{m}^B}\right) + W^B g'(\phi), \tag{9}$$

$$\Psi(\phi,T) = -\frac{P(\phi)}{T^2}(L^A - L^B). \tag{10}$$

In the above equations, $P(\phi)$ should be 0 in solid and 1 in liquid. Here it is chosen to have the form $P(\phi) = \phi^3(6\phi^2 - 15\phi + 10)$. D_T is the thermal diffusivity and C_P is the specific heat. $L^{A,B}$ and $T_\mathrm{m}^{A,B}$ are the latent heat per unit volume and the melting temperature of the pure component A and B. $W^{A,B}$ is the well height. The solute diffusivity is defined as $D_c = D_\mathrm{L}P(\phi) + D_\mathrm{S}(1-P(\phi))$, D_L and D_S being the diffusivities in the liquid and in the solid respectively. M_c depends upon c and ϕ as $M_c = \frac{v_\mathrm{m}}{R}c(1-c)D_c$, where v_m is the molar volume and R is the gas constant. The model parameters M_ϕ, ε, W depend on the physical properties of the alloy components.[5]

2.2. Computational issues

The phase-field model developed in Sec. 2.1 is used to study the solidification of highly undercooled $Ni_{50}Cu_{50}$ (at.%) alloy. The physical data is summarized in Table 1, in which σ and η are surface tension and interface kinetic coefficient respectively. Equations (5)–(7) have been considered two dimensional under fluxless boundary conditions $\phi_x = c_x = T_x = 0$ at the domain's walls. The equations are discretized using a finite difference scheme. Then, an explicit scheme is employed to advance the phase field and concentration equations. The temperature equation is solved by an alternating direction implicit (ADI) scheme, which is unconditionally stable. The solvability of the phase field and concentration equations requires the time step Δt to be subject to a Courant type stability condition of the form: $\Delta t \le \Delta x^2/5D$, where $D = D_\mathrm{L}$ or $D = M_\phi\varepsilon^2$, and Δx is the spacial step which is chosen equal to the interface thickness δ, δ=1×10^{-6}cm.

Due to the quite different length scales involved in the solidification process, the computational domain is divided into two parts: an inner region for the phase and concentration fields, and an outer region, where only the temperature equation is solved. The inner region is fixed 25μm×25μm. But the outer region is changeable. The smaller the undercooling, the bigger is the outer region in order to keep the boundary walls at the initial temperature constantly.

Table 1. Material parameters for the Ni-Cu alloy.[9,10]

parameter	T_m/K	L/ J·cm^{-3}	D_L/cm^2·s^{-1}	D_S/cm^2·s^{-1}	D_T/cm^2·s^{-1}	σ/ J·cm^{-2}	η/cm·s^{-1}K^{-1}	C_P /J·cm^{-3}K^{-1}
Ni	1728	2350						
$Ni_{50}Cu_{50}$			3.33×10^{-5}	3.33×10^{-9}	0.11	3.84×10^{-5}	140	4.878
Cu	1538	1728						

3. Results and discussion

3.1. Dendrite morphologies at different undercoolings

Figure 1 shows the dendrite pattern evolution at different undercoolings. At lower undercooling (Fig.1(a)), the secondary arms are not well developed. With increasing undercooling (Fig.1(b)), the secondary arms on the two primary stalks compete with each other, and some of them advance into the undercooled liquid, obtaining more growth space and driving force. The ternary arms are also formed. A well-developed dendrite is obtained after a longer solidification time. As the undercooling is increased near the hypercooling (L/C_P) (Fig.1(c)), which is about 428K for $Ni_{50}Cu_{50}$, the dendrite pattern changes greatly. The primary trunk and the arms of various orders become very thick. More importantly, the ternary arms are on longer perpendicular to the secondary arms, but tend to grow in the direction of heat flow, which is normal to the outline of the dendrite surface.[11] As the undercooling is beyond the hypercooling (Fig.1(d), (e)), the crystal becomes compact grain rather than fractal dendrite. It acquires a diamond like shape with a number of cells on its surface. The interface perturbations are now referred to as cells but not as secondary arms because they do not grow in the preferred crystallographic direction which is orthogonal to the axis of the primary trunk, whereas

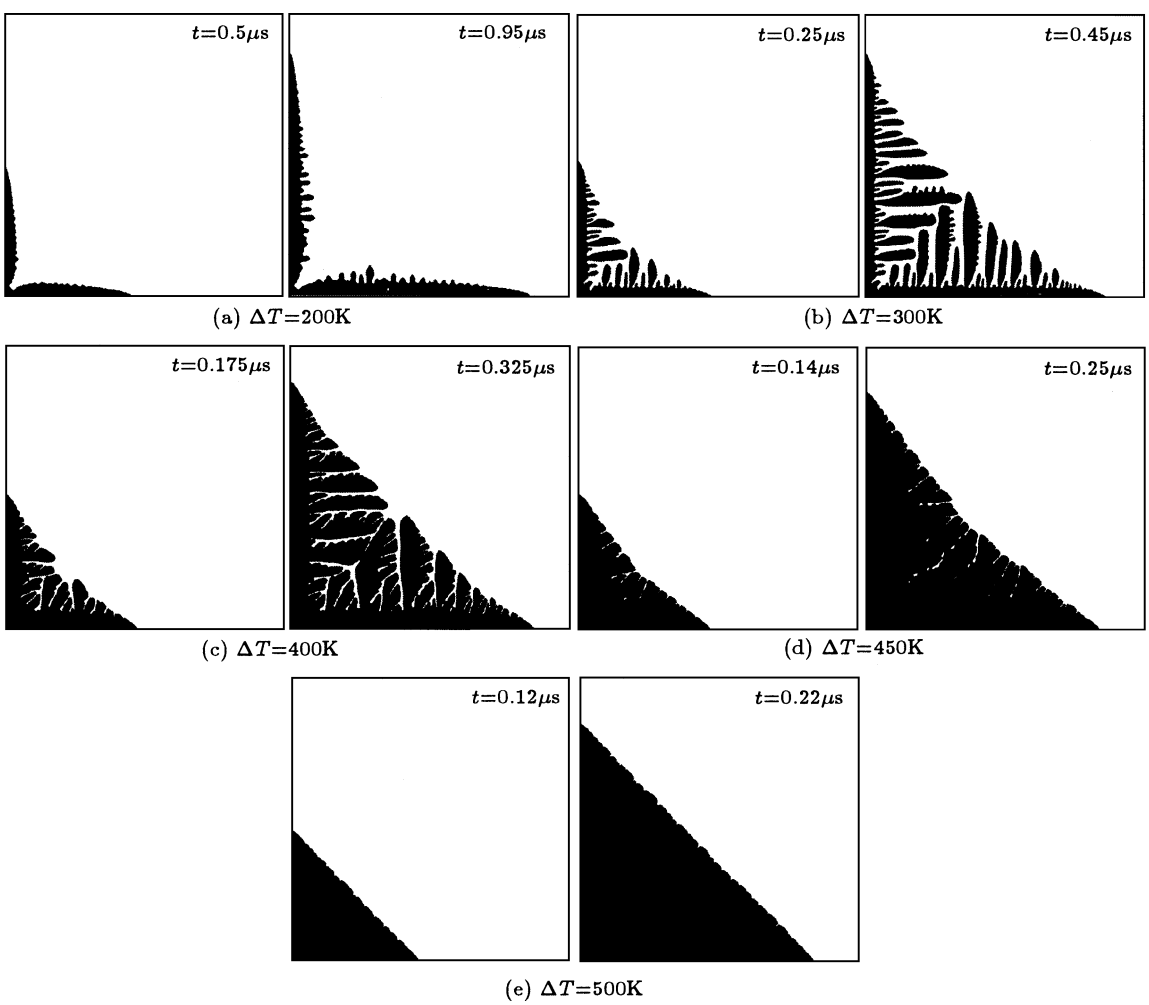


Fig.1. Morphology evolution at different undercoolings.

they grow with axes parallel to the heat flow directions. The reason for this phenomenon is that at high undercooling solute trapping takes place and solidification is dominantly controlled by heat extraction. The temperature gradient along the heat flow direction is so high that the anisotropy of the crystal is suppressed severely.

Grujicic *et al*[12] have modelled the rapid solidification of a binary alloy at high cooling rates and obtained a similar conclusion with regard to the influence of cooling rate on dendrite morphology.

3.2. Concentration and temperature distribution

Because of the large undercoolings adopted in this work, the solute trapping occurs in most of the cases. The plots of the concentration profiles are nearly unintelligible. Only two representative plots are presented here (Fig.2), which correspond to the right-hand pictures in Fig.1(b, e). It is noted that the concentration range at an undercooling of 500K is much narrower than that at an undercooling of 300K because of the larger growth rate and the severer solute trapping effect.

From the temperature profiles (Fig.3) which correspond to the right-hand pictures in Fig.1(a,b,c,e), it can be seen that the larger the undercooling, the shorter the heat diffusion layer and the higher the temperature gradient. It can also be observed that the highest temperatures are generally related with pockets of liquid which are being cut off from the rest of the liquid.

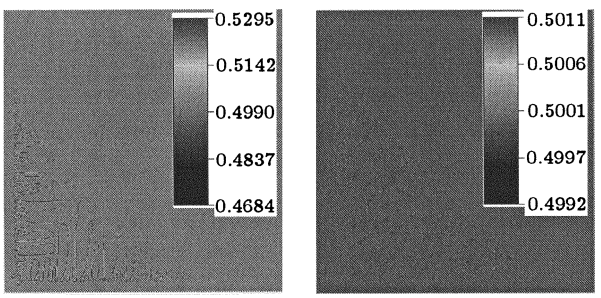


Fig.2. Concentration profiles at different undercoolings.

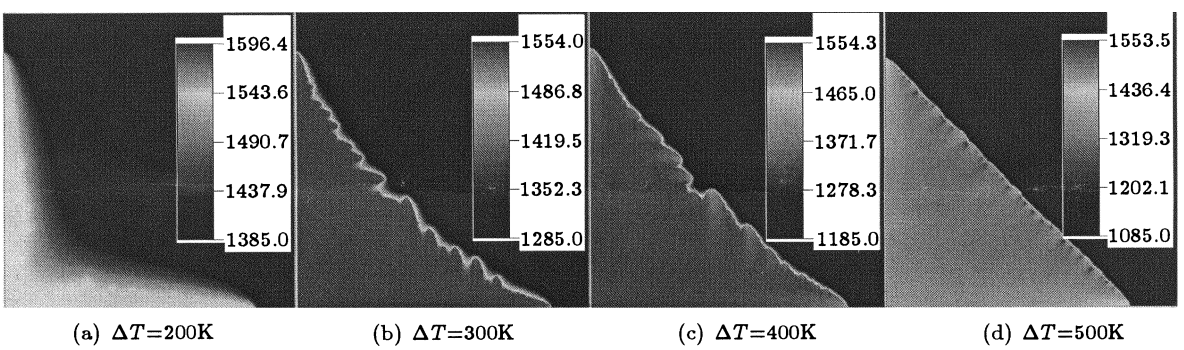


Fig.3. Temperature profiles at different undercoolings.

3.3. Quantitative analysis

The tip radius R and growth velocity V are two important parameters in crystal growth . They are determined from the calculated phase field using the method of Wheeler.[13] The evolution of both R and V under different conditions is tracked to ensure that a steady state has been achieved and when this is the case, values of R and V for the simulation are calculated by averaging over about 10^4 time steps. The behaviours of R and V as functions of ΔT are shown in Figs.4 and 5 respectively. With increasing undercooling, the tip radius changes in the following manner: decrease $\rightarrow$ increase $\rightarrow$ decrease, while the growth velocity increases monotonically.

According to BCT model, the total undercooling at the dendrite tip consists of four contributions:

$$\Delta T = \Delta T_{\mathrm{t}} + \Delta T_{\mathrm{c}} + \Delta T_{\mathrm{k}} + \Delta T_{\mathrm{r}} \tag{11}$$

where ΔT_{t}, ΔT_{c}, ΔT_{k}, ΔT_{r} are the thermal undercooling, the solutal undercooling, the interfacial kinetic undercooling and the curvature undercooling, respectively. They can be expressed as follows:

$$\Delta T_{\mathrm{t}} = T^* - T_\infty, \quad \Delta T_{\mathrm{c}} = mc_0 - m^* c_L^*,$$

$$\Delta T_{\mathrm{k}} = \frac{V}{\mu}, \quad \Delta T_{\mathrm{r}} = \frac{2\Gamma}{R}$$

where T^*—dendrite tip temperature, T_∞—far-field temperature, c_0—nominal composition of the alloy, m—equilibrium liquidus slope, m^*—growth-velocity-dependent nonequilibrium liquidus slope, c_L^*—solute

(Cu) concentration of the liquid at the dendrite tip, μ—interface kinetic coefficient, Γ—Gibbs–Thomson parameter.

In the present work, ΔT_t, ΔT_c, ΔT_k at different undercoolings are determined from the simulation results directly and are shown in Fig.6. Because ΔT_r is much smaller than other terms, it is omitted here.

At low total undercooling, the solutal undercooling is greater than the thermal undercooling, and the dendrite growth is mainly controlled by the solute diffusion. In this region, the dendrite tip radius decreases with the total undercooling so as to satisfy the requirement of solute diffusion. As the undercooling continues to increase, the solutal undercooling reaches its maximum and begins to drop, but the thermal undercooling rises quickly and exceeds the solutal undercooling. This indicates the transition from solutal diffusion to thermal diffusion controlled growth, which makes the tip radius begin to increase. As the undercooling increases further, the interface kinetic effect becomes strong and goes beyond the solutal contribution. The various undercooling contributions comprehensively make the tip radius decrease again. It is noted that the thermal undercooling is much larger than other contributions, which is responsible for the compact growth patterns at undercoolings over 400K in Fig.1(d,e).

Li *et al*[14] have solved the BCT model analytically for the alloy $Ni_{50}Cu_{50}$, obtaining the values of R, V, ΔT_t, ΔT_c, ΔT_k, ΔT_r. The details can be found in Ref.[14]. Comparison between the numerical results in this work with the BCT analytical results in Ref.[14] shows that they agree qualitatively with each other.

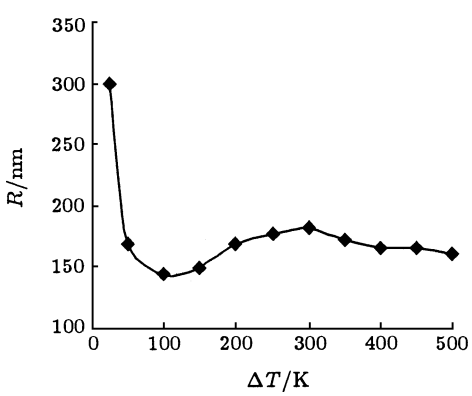


Fig.4. Dentrite tip radius vs. undercooling.

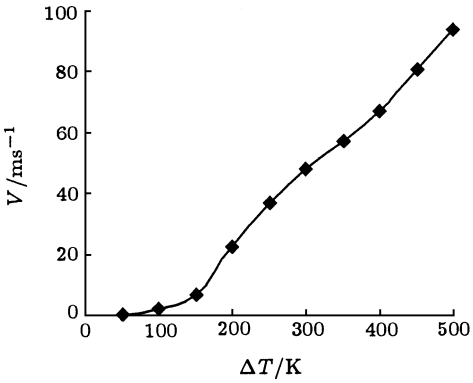


Fig.5. Growth velocity vs. undercooling.

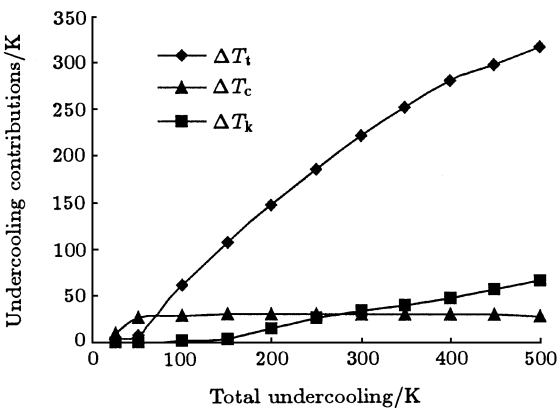


Fig.6. Undercooling contribution vs. total undercooling.

4. Conclusion

The crystal growth into undercooled alloy melts is studied through non-isothermal phase-field simulation. With increasing undercooling, the dendrite morphology changes from poorly developed dendrite, via the well-developed dendrite containing secondary and ternary arms, to the compact diamond-shaped grain. The tip radius, the growth rate and the solutal, thermal, kinetic undercooling contributions are determined directly from the simulation results. The tendency of change of these parameters with initial undercoolings is consistent with that predicted by the BCT model. It is shown that the dendrite growth transits from solutal diffusion controlled to thermal diffusion controlled growth as the undercooling increases.

References

[1] Lipton J, Glicksman M E and Kurz W 1984 *Mater. Sci. Eng.* **65** 57

[2] Lipton J, Kurz W and Trivedi R 1987 *Acta Metall. Mater.* **26** 1681

[3] Boettinger W J, Coriell S R and Trivedi R 1988 *Rapid Solidification Processing: Principles and Technologies* IV (Claitor's, Baton Rouge, LA) p13

[4] Nestler Britta and Wheeler Adam A 2002 *Comput. Phys. Commun.* **147** 230

[5] Warren J A and Boettinger W J 1995 *Acta Metall. Mater.* **43** 689

[6] Mullis A M 2003 *Acta Mater.* **51** 1959

[7] Li M E, Yang G C and Zhou Y H 2005 *Acta Phys. Sin.* **54** 454 (in Chinese)

[8] Conti M 1998 *Phys. Rev.* E **58** 6166

[9] Willnecker R, Herlach D M and Feuerbacher 1989 *Phys. Rev. Lett.* **62** 2707

[10] Brandes E A (Ed.) 1983 *Smithells Metals Reference Book* 6th edn (London: Butterworths)

[11] Wu Y, Piccone T J, Shiohara Y and Flemings M C 1987 *Metall. Trans.* **18A** 915

[12] Grujicic M, Gao G and Miller R S 2002 *J. Mater. Synth. Process.* **10** 191

[13] Wheeler A A, Murray B T and Schaefer R J 1993 *Physica* D **66** 243

[14] Li J F, Yang G C and Zhou Y H 1998 *Mater. Res. Bull.* **33** 141